Role of methane in ammonia combustion in air: From microscale to macroscale

Jing Wang [a], Fuquan Huang [a], Xinyan Wang [b], Xi Zhuo Jiang [a,*], Kai H. Luo [c]

[a] School of Mechanical Engineering and Automation, Northeastern University, Shenyang 110819, China
[b] Centre for Advanced Powertrain and Fuels, Brunel University London, Uxbridge UB8 3PH, United Kingdom
[c] Department of Mechanical Engineering, University College London, Torrington Place, London WC1E 7JE, United Kingdom

ABSTRACT

Ammonia (NH_3) has gained increasing recognition as a carbon-free fuel. To enhance NH_3 combustion, reactive gases, like methane (CH_4), are usually added to the combustion system. In this work, the role of CH_4 in NH_3 combustion is systematically studied. A series of reactive force field molecular dynamic (ReaxFF MD) simulations are implemented to investigate effects of CH_4 addition on the consumption of NH_3 and the yields of nitrogen oxides (NO_x) from the atomic perspective: CH_4 accelerates the consumption of NH_3 by shortening the decomposition time of the first NH_3 molecule and increasing the translational kinetic energy of the system; CH_4 modifies the yield of NO_x by complicating the elementary reactions and introducing additional intermediates. The fuel ratio of CH_4 and NH_3 between 0.5 and 1 is suggested for a cleaner and enhanced NH_3 combustion. By summarising the findings from the latest publications and the present work, the role of CH_4 in NH_3 combustion is comprehensively analysed from the macroscale and microscale perspectives: CH_4 accelerates the progress of NH_3 combustion flame, activates chemical reactions, and aggravates NO_x emissions at a low CH_4 content. Taking the NH_3/CH_4 combustion as an example, this study provides an exclusive perspective to understand combustion phenomena from the microscale events to macroscale observations.

1. Introduction

Ammonia (NH_3) is increasingly recognized as a green and sustainable fuel in resolving the global carbon emission issues. NH_3 is a promising hydrogen carrier, but the low flame speed and high auto-ignition temperature limits its wide applications for direct usage in power systems [1]. Previous research showed that by adding auxiliary gases/fuels, like methane (CH_4) [2], to the NH_3 combustion system, the combustion performance of NH_3 can be effectively improved.

Various aspects of NH_3/CH_4 combustion were reported in previous studies. Okafor et al. [3] pointed out that high CH_4 volume fraction increases the flame speed in micro gas turbine. Henshaw et al. [4] and Kurata et al. [5] reported a nonlinear relation between the content of CH_4 and NO_x formation in NH_3/CH_4 combustion. Li et al. [6] measured the yields of NO_x, CO, and CO_2 in NH_3/CH_4 combustion under different equivalent ratios. Skreiberg et al. [7] analysed the combustion products of NH_3/CH_4 under the actual working condition (1400 K) and pointed out that different reaction conditions would influence the types of products.

Kinetic models for modelling NH_3/CH_4 combustion under varying conditions have also been a hot topic for researchers. Early mechanisms included Konnov's mechanism [8], GRI-Mech 3.0 mechanism [9], Mendiara's mechanism [10] and Tian's mechanism [11]. Accuracy of these reaction mechanisms were reviewed in Ref. [12]. Afterwards, mechanisms with more accurate predictions for certain species, reduced mechanisms and mechanisms for specific conditions were successively proposed. For example, Okafor et al. [13] simulated the flame characteristics of NH_3/CH_4 combustion, and pointed out the large deviations in the prediction of laminar flame speed and NO generation by Tian [11] and GRI Mech 3.0 mechanisms [9]; the researchers then developed a set of reaction mechanism that can produce more accurate predictions in flame speed and NO generation. Li et al. [14], Jiang et al. [15] and Mikulčić et al. [16] reduced the NH_3/CH_4 mechanisms for different combustion conditions. Shu et al. [17] proposed a reaction mechanism for NH_3/CH_4 combustion particularly for high pressure conditions.

Reactive force field molecular dynamics (ReaxFF MD) simulations play an indispensable role in manifesting the performance of NH_3 combustion. Guo et al. [18] studied the co-combustion behaviour of

Table 1
Cases in the present study.

Case	T, K	Numbers of NH₃/CH₄/O₂/N₂	α	Side length, Å
1	3000	20/0/200/780	0	199.92
2	3000	20/2/200/780	0.1	200
3	3000	20/5/200/780	0.25	200.11
4	3000	20/10/200/780	0.5	200.29
5	3000	20/20/200/780	1	200.66
6	3000	20/40/200/780	2	201.41
7	3000	20/60/200/780	3	202.14
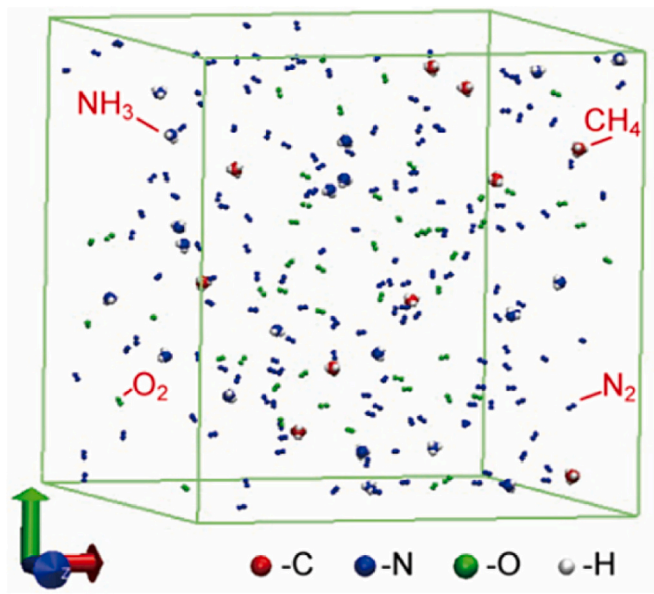
Fig. 1. Initial configuration of the NH₃/CH₄/N₂/O₂ system.

NH₃/CH₄ at different temperatures, CH₄ mixing ratio and O₂ equivalence ratios. Zhang et al. [19] investigated the effects of CH₄ reactivity on NH₃ oxidation in an O₂/N₂ environment. In our previous study [20], the ReaxFF MD method was used to scrutinise the behaviours of the reacting molecules/radicals, and reaction pathways at high temperatures and pressures were proposed by tracking the atomic trajectories. The reaction pathways proposed by the ReaxFF MD method were compared with popular kinetic models, and new pathways and intermediates were identified. According to our previous study, the addition of CH₄ could lower the activation energy of NH₃ combustion and thus accelerate the consumption of NH₃. Yet, how the CH₄ could modify the NH₃ combustion chemistry from the atomic perspective has not been clarified in such a study. Additional efforts are still needed to reveal the effects of CH₄ on reaction mechanisms for NH₃ combustion at the atomic level. Indeed, the flame properties of NH₃ combustion observed at the macroscale are intimately related to microscale behaviour of the reacting radicals. However, to our best knowledge, there is no paper by far bridging the gaps between the macroscale observations and the atomic behaviours in NH₃ combustion.

The aim of the present study is to present a thorough understanding of the role of CH₄ in NH₃ combustion from the atomic behaviour to macroscale combustion phenomena. To achieve this goal, we first reveal the effects of CH₄ on microscale mechanisms for NH₃ combustion via a series of reactive force field (ReaxFF) molecular dynamics (MD) simulations. Then, we summarise the latest publications on NH₃/CH₄ combustion. Finally, the macroscale observables and microscale indicators are linked and the role of CH₄ in NH₃ combustion is encapsulated.

2. Methods

2.1. Reactive force field molecular dynamics simulations

The ReaxFF MD is a type of MD method which uses a set of well-trained force field parameters to simulate chemical reactions with acceptable accuracy and computational costs. The potential of an MD system is calculated by the sum of bonded and non-bonded energies, as shown in Eq. (1).

$$E = E_{bonded} + E_{non-bonded}$$

$$= E_{bond} + E_{over} + E_{under} + E_{lp} + E_{val} + E_{tor} + E_{vdWaals} + E_{Coulomb} \tag{1}$$

where E_{bonded} comprises bond energy (E_{bond}), overcoordination energy penalty (E_{over}), undercoordination stability (E_{under}), lone pair energy (E_{lp}), valence angle energy (E_{val}) and torsion angle energy (E_{tor}); $E_{non-bonded}$ includes van der Waals interaction ($E_{vdWaals}$) between atoms and electrostatic energy ($E_{Coulomb}$) [21]. Details about the ReaxFF MD method can be found in Refs. [22, 23].

2.2. Case set-ups

In the present ReaxFF MD simulations, NH₃, CH₄, N₂ and O₂ molecules were randomly placed in a cubic simulation domain with the aid of PACKMOL codes [24]. To study the effects of CH₄ on NH₃ combustion, the number of CH₄ molecules was varied and the numbers of NH₃, N₂ and O₂ were fixed. To facilitate analysis, the fuel ratio of CH₄ and NH₃, α, was defined in Eq. (2).

$$\alpha = \frac{n(CH_4)}{n(NH_3)} \tag{2}$$

where $n(CH_4)$ and $n(NH_3)$ are the numbers of CH₄ and NH₃ molecules, respectively. Herein, α varied from 0 to 3 to mimic NH₃ combustion from a pure NH₃ condition to a mixed gas condition. The cases used in the present study are listed in Table 1.

According to our previous study [20], a high temperature could accelerate reaction rate and significantly reduce computational costs, and thus a temperature of 3000 K was selected in the present study. The same density of molecules at the beginning of the reactions, indicating the same initial pressure, was selected for all simulations as well. To keep a constant density, the side length of the simulation box was slightly changed. A typical initial configuration of the simulation box is demonstrated in Fig. 1. For each case, five simulations with different initial configurations were conducted, and data analysis was implemented based on 35 simulations.

2.3. Simulation details

A C/H/N/O ReaxFF parameter set [25,26] was used in the present system, and the force field parameters file can be found in our previous publication [20]. The ReaxFF parameters were well trained by quantum chemistry and carefully validated by experiments, and its effectiveness and reliability of parameters for calculating systems with C, H, O and N elements were demonstrated in previous studies [20,27,28].

Before reaction simulations, equilibration simulations were performed to minimize the system energy for a physical time of 40 ps at 300 K. The system was then heated from 300 K to 3000 K for 500 ps. Afterwards, the temperature remained constant at 3000 K and the reaction simulation lasted for 8000 ps until NH₃ was fully consumed.

The time step was 0.1 fs, and the bond order cut-off was 0.3 [29]. A canonical (NVT) ensemble with a Nosé–Hoover temperature controlling algorithm was selected for all simulations with a damping constant of 100 fs. The periodic boundary conditions [30] were used in all three directions. All the simulations were implemented with the REAXC package in the LAMMPS (Large-scale Atomic/Molecular Massively
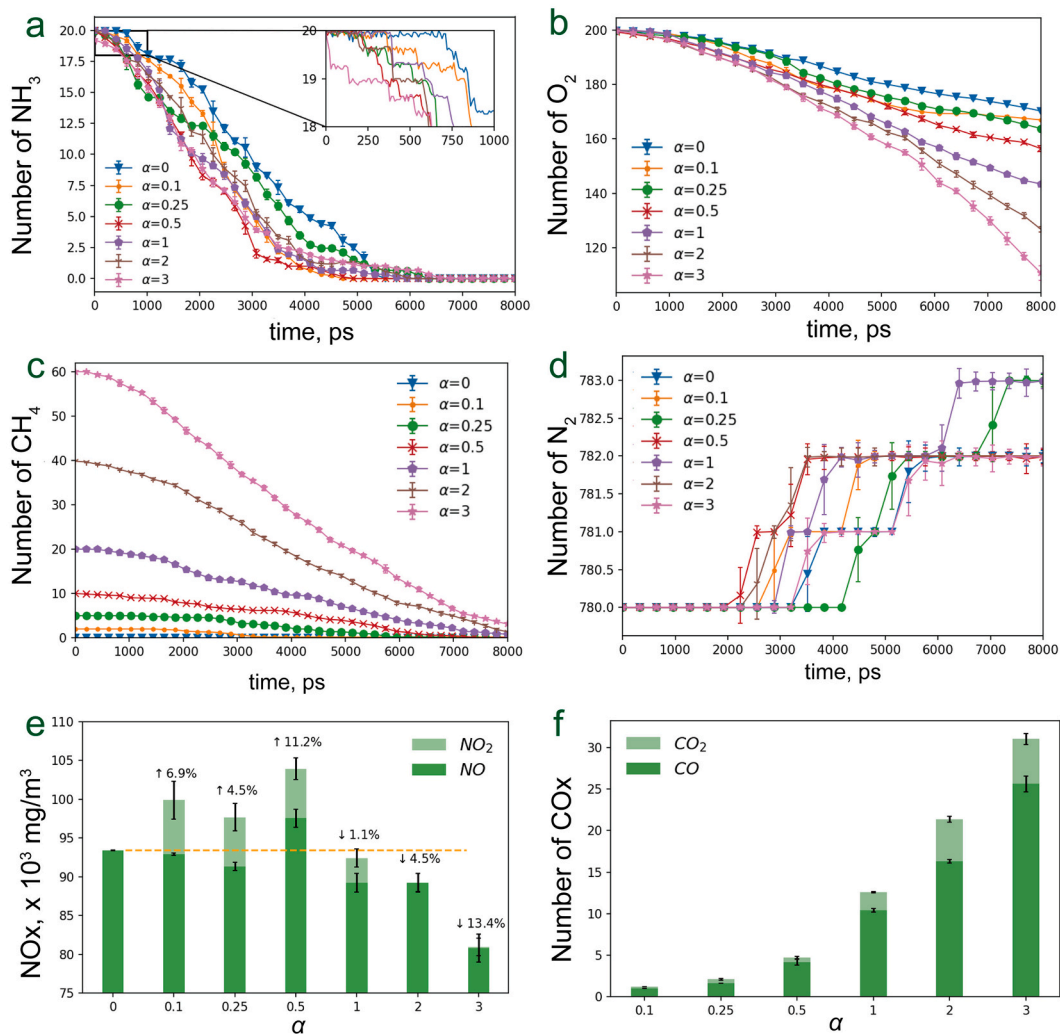
Fig. 2. Effects of CH_4 on NH_3 combustion under different fuel ratios. a. Time evolution of the number of NH_3 (Data were time-averaged every 200 ps). b. Time evolution of the number of O_2. c. Time evolution of the number of CH_4. d. Time evolution of the number of N_2. e. Number of NO_x (NO and NO_2) changes with fuel ratios. f. Number of CO_x (CO and CO_2) changes with fuel ratios.
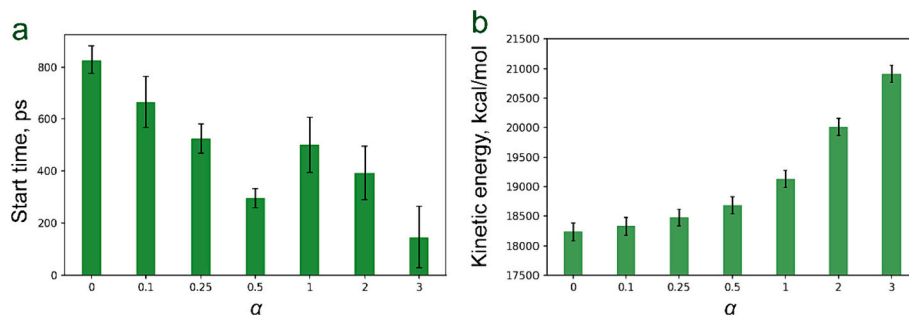
Fig. 3. Reaction start time and kinetic energy. a. The average start time of NH_3 decomposition. b. Kinetic energy of systems under different fuel ratio conditions.
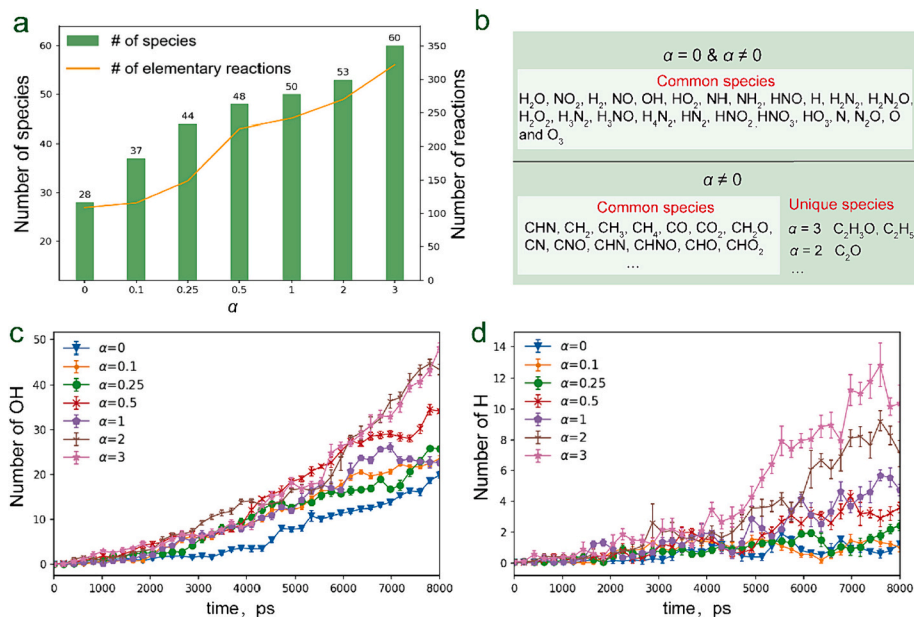
Fig. 4. Intermediates and elementary reactions. a. Numbers of intermediate species and elementary reactions at varying fuel ratio conditions. b. Comparisons of intermediates among cases at different fuel ratio conditions. c. Time evolution of the number of OH radicals. d. Time evolution of the number of H radicals.
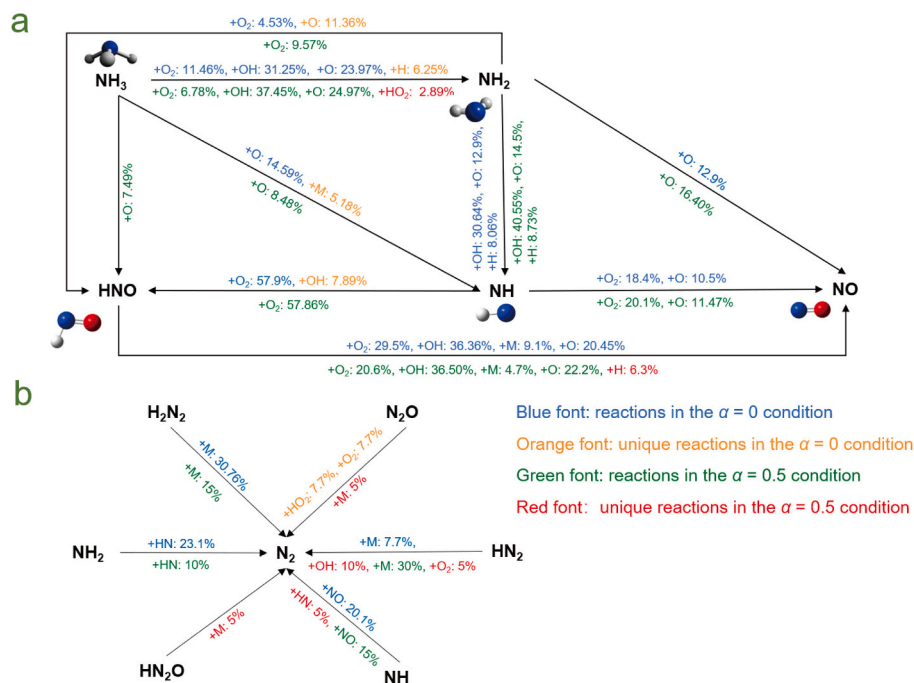
Fig. 5. Comparisons of the representative elementary reactions between NH_3 and NH_3/CH_4 combustion. a. NO formation pathways. b. N_2 formation pathways. Blue font: reactions in the $\alpha = 0$ case, orange font: unique reactions in the $\alpha = 0$ case, green font: reactions in the $\alpha = 0.5$ case, and red font: unique reactions in the $\alpha = 0.5$ case. (For interpretation of the references to colour in this figure legend, the reader is referred to the web version of this article.)
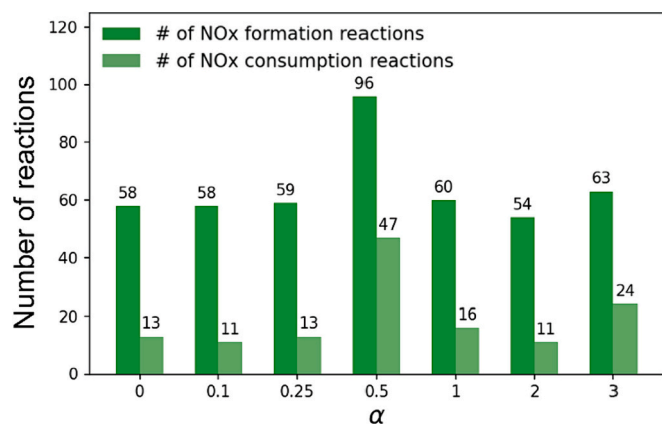
Fig. 6. Numbers of NO_x formation and consumption reaction types.

Parallel Simulator) software [31]. The visualization was conducted in VMD [32]. Post-processing of the MD results was accomplished using in-house PYTHON (Python Software Foundation, Wilmington, De) scripts. The reaction pathways were analysed using the ChemTraYzer [33] script. Unless otherwise indicated, data with error bars represent mean $\pm$ SD (standard deviations).

3. Results and discussion

3.1. Time-evolutions of species, start time of reactions and kinetic energy

The time evolutions of numbers of NH_3 at different fuel ratios are shown in Fig. 2a. As shown in Fig. 2a, the addition of CH_4 accelerates the consumption of NH_3 molecules, which agrees with previous experimental studies [34–37]. The consumption rate of O_2 molecules also increases with α (Fig. 2b), as the oxidation of CH_4 molecules requires additional O_2 molecules as well. Time evolutions of numbers of CH_4 and N_2 are shown in Fig. 2c and d. In the rich O_2 environment, CH_4 is rapidly consumed and N_2 is formed as product of NH_3 combustion.

The numbers of NO_x at the end of reactions were compared among cases of different fuel ratios, as shown in Fig. 2e. A non-linear trend of NO_x generation with the addition of CH_4 was observed: the yield of NO_x reached a peak at $\alpha = 0.5$; afterwards, the addition of CH_4 inhibits the generation of NO_x significantly. The $\alpha = 0.25$ case has the fewer NO_x emissions than those in the cases of $\alpha = 0.1$ and 0.5. The number of reactions relating the formation of NO_x was counted and the number of NO_x formation pathways at $\alpha = 0.25$ is fewer than those in $\alpha = 0.1$ and $\alpha = 0.5$ cases. Such a non-linear trend was also reported in a previous study [38]. The non-linear tread narrows down the content of CH_4 that can be added to the NH_3 combustion: on the one hand, the NO_x emissions should be limited and a larger α value is preferable; on the other hand, the number of carbon oxides (CO and CO_2) increases with α (Fig. 2f) and a smaller α value is favoured. With these considerations, the fuel ratio of CH_4 and NH_3 is suggested to be between 0.5 and 1 for cleaner and enhanced combustion of NH_3.

A scrutiny of the time that the first NH_3 molecule starts to decompose suggests that the addition of CH_4 expedites the NH_3 combustion, as shown in Fig. 3a. For example, in the $\alpha = 0$ case the first NH_3 is consumed at an average instant of 827 ps, whilst in the $\alpha = 3$ case NH_3 starts to consume at as early as 146 ps. The early start time of NH_3 decomposition in the presence of CH_4 was also reported in previous observations [39,40]. In the $\alpha = 3$ case, the earliest NH_3 consumption was observed, which implies a highly reactive state of the system. The highly reactive state may be due to a high content of reactive radicals. Since results at such a CH_4 content were lacking in previous studies, further validation work is still needed. The effects of CH_4 on NH_3

combustion are two-fold: the addition of CH_4 could accelerate the consumption of NH_3 by generating radical s like H; on the other hand, CH_4 could compete with NH_3 to consume O_2 which impedes the consumption of NH_3. In Fig. 3a, when α changes from 0.5 to 1, the consumption of NH_3 is retarded, which may be attributed to the competition for O_2 from CH_4. The kinetic energy of these systems was also calculated. The kinetic energy of the system was calculated from the temperature of the system with $1/2 k_B T$ of energy for each degree of freedom. Fig. 3b shows kinetic energy of the system increases with the addition of CH_4, accounting for the accelerated NH_3 consumption in the presence of CH_4 in Fig. 2a.

3.2. Intermediates and elementary reactions

The numbers of intermediates and elementary reactions under different fuel ratio conditions are illustrated in Fig. 4a. Both the numbers of intermediate species and reaction pathways increase with the fuel ratio, indicating that the addition of CH_4 complicates the NH_3 combustion as it accelerates the reaction.

Furthermore, the species of intermediates were compared among different fuel ratio conditions. Common intermediates among these cases and unique intermediates in each situation were identified. As shown in Fig. 4b, H_2O, NO_2, H_2, NO, OH, HO_2, NH, NH_2, HNO, H, H_2N_2, H_2N_2O, H_2NO, H_2O_2, H_3N, H_3N_2, H_3NO, H_4N_2, HN_2, HNO_2, HNO_3, HO_3, N, N_2O, O and O_3 are broadly shared among cases with and without the addition of CH_4. The addition of CH_4, on the other hand, produces carbon-containing species. The common carbon-containing species were listed in Fig. 4b. Fig. 4b also suggests that the varieties of the carbon-containing species differ when the fuel ratio is changed. For example, C_2H_3O and C_2H_5 were only observed in the $\alpha = 3$ cases while C_2O was only produced in the $\alpha = 2$ case. The variations in species at different fuel ratio conditions further suggest that the presence of CH_4 modifies the reaction mechanisms as it enhances the combustion of NH_3.

Among all the intermediates and radicals, hydrogen atom (H) and hydroxyl (OH) were observed most frequently. Time-evolutions of the numbers of H and OH radicals under different fuel ratio conditions were investigated, as shown in Fig. 4c and d, respectively. OH is the predominant radical in the NH_3/CH_4 combustion. Reaction pathways for the generation of OH radicals include $CH_4 + O \rightarrow CH_3 + OH$ and $CH_3 + O \rightarrow CH_2 + OH$. As more CH_4 molecules are added to the combustion system, more OH radicals are produced as shown in Fig. 4c. CH_4 is a source of H atoms, and the number of H radicals increases rapidly at a high α value, as shown in Fig. 4d. Reaction pathways for the formation of H radicals with the addition of CH_4 include $CH_3 + O \rightarrow CH_2O + H$, $CHO_2 \rightarrow CO_2 + H$, $CHO \rightarrow CO + H$ and $CO + OH \rightarrow CO_2 + H$.

To further reveal how CH_4 modifies the reaction mechanisms of NH_3 combustion, the reaction pathways leading to the formation of NO and N_2 were compared between the pure NH_3 combustion (i.e., the $\alpha = 0$ case) and the NH_3/CH_4 mixed combustion (The $\alpha = 0.5$ case was used). In Fig. 5, colour fonts were used to distinguish whether the reaction was from the $\alpha = 0$ or $\alpha = 0.5$ case; the digitals represent the probabilities that individual elementary reactions occur among all the elementary reactions. As shown in Fig. 5a and b, the reaction channels and the probabilities individual elementary reactions occur can be completely different, although common intermediates were formed between the pure NH_3 combustion and the mixed gas combustion. For example, NH_3 can be directly converted to HNO in the $\alpha = 0.5$ case, whilst NH_2 should be formed before HNO in the $\alpha = 0$ case; O_2, OH and O radicals could all react with NH_3 in the $\alpha = 0$ and $\alpha = 0.5$ cases, however, the probabilities of detecting these elementary reactions vary when α changes.

3.3. Reaction pathways of NO_x

To reveal the mechanism for the effects of CH_4 on NO_x emissions, the reaction pathways were scrutinized. The numbers of NO_x formation and

Table 2
NO_x-related elementary reactions at different fuel ratio conditions.

No.	Elementary reactions	α						
		0	0.1	0.25	0.5	1	2	3
R1	$HNO + OH \rightarrow NO + H_2O$	•	•	•	•	•	•	•
R2	$HNO + O_2 \rightarrow NO + HO_2$	•	•	•	•	•	•	•
R3	$HNO + O \rightarrow NO + OH$	•	•	•	•	•	•	•
R4	$NO_2 \rightarrow NO + O$	•	•	•	•	•	•	•
R5	$N + O_2 \rightarrow NO + O$	•	•	•	•	•	•	•
R6	$NH_2 + O \rightarrow NO + H_2$	•	•	•	•	•	•	•
R7	$H + NO_2 \rightarrow NO + OH$	•	•	•	•	•	•	•
R8	$NH + O \rightarrow NO + H$	•	•	•	•	•	•	•
R9	$NH + O_2 \rightarrow NO + OH$	•	•	•	•	•	•	•
R10	$HNO_2 \rightarrow NO + OH$	•	•	•	•	•	•	•
R11	$HNO + H \rightarrow NO + H_2$	•	•	•	•	•	•	•
R12	$HNO \rightarrow NO + H$	•		•	•	•	•	•
R13	$HO_2 + NO \rightarrow NO_2 + OH$	•	•		•	•	•	•
R14	$HNO + HO_2 \rightarrow NO + H_2O_2$		•		•	•	•	•
R15	$H_2NO \rightarrow NO + H_2$	•	•		•		•	•
R16	$H + NO_2 \rightarrow NO + OH$	•	•	•	•	•		
R17	$HNO + NH_2 \rightarrow NO + NH_3$			•	•	•		
R18	$O + NO_2 \rightarrow NO + O_2$					•	•	•
R19	$N + OH \rightarrow NO + H$	•				•	•	•
R20	$CNO + O \rightarrow NO + CO$						•	•
R21	$HNO + NO_2 \rightarrow NO + HNO_2$	•						
R22	$H_2NO + O_2 \rightarrow NO + H_2O_2$	•						
R23	$NH + O_2 \rightarrow NO_2 + H$	•						
R24	$NO_2 + OH \rightarrow NO + HO_2$		•					
R25	$HNO_2 + O_2 \rightarrow NO_2 + HO_2$		•					
R26	$HNO + O \rightarrow NO_2 + H$			•				
R27	$NH_2 + N_2O \rightarrow NO + N_2 + H_2$			•				
R28	$NO + O_2 \rightarrow NO_2 + O$				•			
R29	$HNO + O_2 \rightarrow NO_2 + OH$				•			
R30	$H_2 + NO_2 \rightarrow NO + H_2O$				•			
R31	$HNO_2 + OH \rightarrow NO_2 + H_2O$				•			
R32	$H_2 + N_2O \rightarrow NO + NH_2$				•			
R33	$H_2 + NO_2 \rightarrow NO + H_2O$				•			
R34	$CO + NO_2 \rightarrow NO + CO_2$					•		
R35	$CN + O_2 \rightarrow NO + CO$					•		
R36	$HNO_2 + H \rightarrow NO + H_2O$						•	
R37	$NH_2 + O \rightarrow NO + H + H$						•	
R38	$HNO + CH_2 \rightarrow NO + CH_3$							•
R39	$HNO + H_2O \rightarrow NO + H_2 + OH$							•
R40	$NH_3 + O_2 \rightarrow NO + H_2O + H$							•
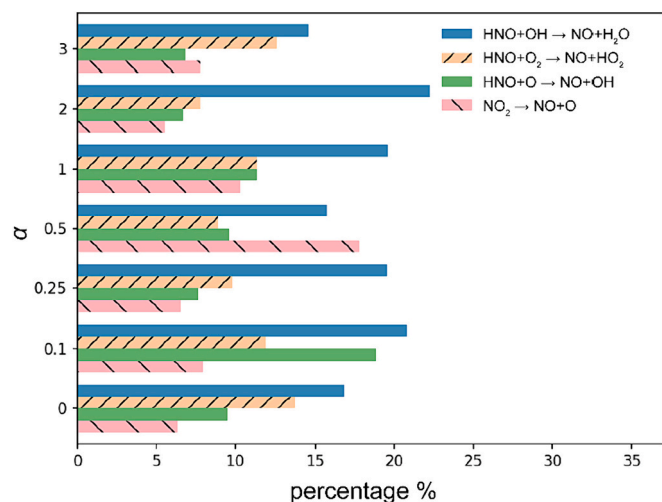
Fig. 7. Probabilities for four principal NO_x-related reactions at different fuel ratio conditions.

consumption reactions were counted, as shown in Fig. 6. The yield of NO_x depends on the difference in fluxes between the formation and the consumption reactions. As shown in Fig. 6, the difference between the numbers of NO_x formation and consumption first increases until α reaches 0.5 and drops afterwards, which explains for the trend of NO emissions in Fig. 2e.

The elementary reactions relating to the formation and consumption of NO_x were further examined, and forty elementary reactions that frequently occurred were listed in Table 2. Common and unique reactions at different fuel ratio conditions were identified. As shown in Table 2, more reaction pathways for the production of NO than those of NO_2 were observed, which explains the number distribution of NO_x in Fig. 2e (more NO molecules than NO_2 were observed in Fig. 2e). As revealed by Table 2, carbon-containing radicals can participate in NO formation directly when α is >1 (R20, R34, R35 and R38). Notably, prompt NO_x is formed in the $\alpha = 3$ case (R38).

R1 ~ R4 in Table 2 were four most frequently observed reactions for NO formation. The probabilities that individual reactions occur were quantified by calculating the proportions of reaction frequency of each elementary reactions to the aggregate reaction frequencies of all the reactions. As shown in Fig. 7, the probability of individual reactions varies with the CH_4 content. In Fig. 7, the proportion of $HNO + O_2 \rightarrow NO + HO_2$ decreases when CH_4 is added to the NH_3 combustion. CH_4 may compete with NH_3 to consume O_2, which inhibits the conversion from HNO to NO in the $HNO + O_2 \rightarrow NO + HO_2$ reaction.

4. Discussion – role of CH_4 in NH_3 combustion in air: from the microscale to macroscale

In the past five years, an increasing number of research papers have been published to discuss the combustion properties of NH_3 as an alternative energy vector to fossil fuels. Herein, we have collected the latest papers about the effects of CH_4 on NH_3 combustion and categorised these references in terms of scales (either microscale or macroscale) in Table 3.

As listed in Table 3, the properties or terminologies usually discussed in macroscale studies of NH_3/CH_4 combustion include ignition delay time or ignition enhancement, laminar flame speed, flammability limit, combustion rate, adiabatic flame temperature, flame propagation, NO_x emissions, flame stability, combustion efficiency and chemical kinetics, just name a few. Such macroscale observations or properties could all be

understood from the microscale behaviour of atoms, molecules and radicals as revealed by the present study and related work by our group [20]. For example, the ignition delay time usually discussed in the macroscale studies is related to the start time that the first NH_3 molecule is decomposed; the laminar flame speed relies on microscale properties like kinetic energy and collision frequency (both affecting the reaction rate); the microscale understandings of the chemical kinetics are indeed the reaction pathways formed by tracking the trajectories of atoms/molecules/radicals. To bridge the gap between macroscale and microscale understandings, a diagram linking the macroscale observations and their corresponding microscale events was proposed, as shown in Fig. 8a.

Considering all the macroscale and microscale findings available, the role of CH_4 in NH_3 combustion in air is summarised in Fig. 8b: CH_4 accelerates the progress of flame, activates chemical reactions, and aggravates NO_x emissions when the CH_4 content is low.

5. Conclusion

In this study, a series of ReaxFF MD simulations were conducted to simulate the NH_3/CH_4 combustion in air under different fuel ratio conditions. The results suggest that the addition of CH_4 enhances the combustion of NH_3 by reducing the start time of NH_3 decomposition and increasing the kinetic energy of systems. CH_4 can inhibit NO_x emissions at a higher content of CH_4 ($\alpha > 1$) but aggravate NO_x emissions at a lower CH_4 content. The fuel ratios of CH_4 and NH_3 between 0.5 and 1 (i.e., $0.5 < \alpha < 1$) are suggested to achieve cleaner and enhanced NH_3 combustion. To better understand the reaction mechanism, the intermediates and reaction pathways were revealed. The presence of CH_4 complicates NH_3 combustion by introducing additional intermediates and reaction pathways, leading to the formation of NO_x were compared among different fuel ratio conditions. By summarising the latest publications of NH_3/CH_4 combustion in air, together with the findings revealed by the present work, the role of CH_4 in NH_3 combustion in air was summarised: CH_4 is an accelerator for the progress of NH_3 combustion flame, an activator for the combustion reactions and an aggravator for NO_x emissions when a low content of CH_4 is added to the combustion system.

The present study provides a comprehensive understanding of the effects of CH_4 on NH_3 combustion. Practical suggestion regarding the content of CH_4 addition is provided. In future work, the activation energy of individual elementary reactions will be calculated to form a complete set of reaction mechanisms for NH_3/CH_4 combustion and to facilitate the prediction of the combustion behaviour.

Declaration of competing interest

The authors declare that they have no known competing financial interests or personal relationships that could have appeared to influence the work reported in this paper.

Data availability

Data will be made available on request.

Table 3
Recent papers on effects of CH_4 on NH_3 combustion.

Category		Year	Conditions	Highlights	Refs.
Macroscale	Flame properties	2023	450, 500 K / 0.8–1.1 MPa	The addition of 10% CH_4 can improve the pure combustion performance, including improving *flame propagation*, shortening *ignition delay* and *combustion duration*, and increasing the average pressure rise rate, but the enhancement effect on combustion is relatively weak when the addition of 10% CH_4 continues to increase to 20%.	[41]
		2021	298 K / 0.1 MPa	As CH_4 is added, the *heat release rate* of NH_3 and the *laminar flame speed* increase.	[42]
		2021	298 K / 1–5 bar	A strong linear correlation between *laminar flame speed* and CH_4 volume fraction. The *flammability limit* varies almost linearly with the CH_4 content. The *adiabatic flame temperature* increases with CH_4 proportion.	[43]
		2021	295 K / 1.0 MPa	Co-combustion with CH_4 further successfully improved the flame stability and combustion efficiency of the liquid NH_3 spray.	[44]
		2020	1300–1900 K / 1–10 atm	The addition of CH_4 additives improves the *ignition* of NH_3.	[39]
		2020	930 to 1140 K / 20 to 70 bar	CH_4 shows strong ignition enhancement to NH_3; at higher CH_4 ratios, the *ignition delay time* approaches that of pure CH_4 and the ignition enhancement tends to level off.	[40]
		2020	298 ± 3 K / 1 atm	The *laminar flame velocity* and *adiabatic flame temperature* increase with CH_4 content.	[45]
		2020	300 K / 0.1 MPa	Flame sustainability to high stretch rate, temperature, *heat release rate* and important *intermediate radicals* of the flames, *carbon oxides and nitrogen oxides* emissions increase with the CH_4 content in the NH_3/CH_4 fuel blends.	[46]
		2019	363 K – 413 K / 1 atm	*Laminar combustion rate* is almost linear with the molar fraction of NH_3 and CH_4.	[47]
	NO$_x$ emissions	2022	300 K / 1 atm	Using of NH_3/CH_4 blends extends the stable operational range of the system, in terms of both working temperatures and equivalence ratios, with respect to pure NH_3. On the other hand, blends produce higher *NO$_x$ emissions*, with respect to both the pure NH_3 and CH_4 cases.	[38]
		2021	500–3000 K / 0.5 MPa	The relationship between *NO emission* and NH_3/CH_4 concentration is nonlinear.	[48]
		2021	1–3 bar	At higher NH_3/CH_4 ratios, *NO emissions* are suppressed as the reduction in free radical mass fraction facilitates the NO reduction reaction.	[49]
		2021	900–1100 K / 20, 40 bar	The *emissions of CO and NO$_x$* increase with the increasing CH_4 content in the fuel mixture.	[17]
		2021	400–500 °C / 0.25 MPa	Higher combustor inlet temperature and CH_4 fuel content reduce *NO$_x$ emissions*.	[50]
		2021	300 K / 1 atm	NH_3 *flame properties* can be promoted through adding a small amount of CH_4 without increasing the NO$_x$ emission level. For the 10% CH_4 flames, *NO emission* is higher than that of the NH_3 flames when equivalence ratio < 1.05. At fuel rich condition, NO emission seems to reach the same amount as the NH_3 flames.	[51]
		2020	300–500 K / 0.10 – 0.50 MPa	Compared to rich-lean pure NH_3 combustion, the addition of CH_4 increases the *flame speed* and reduces *nitrogen oxides* in the secondary combustion zone.	[3]
	Chemical kinetics	2021	293–1500 K	The research simulated carbon chemistry with Konnov, Okafor and San Diego mechanisms, and showed that San Diego mechanism proved to be the best in terms of emissions, especially in terms of *NO emissions*.	[16]
		2020	298 K / 0.1 MPa	A shortened San Diego mechanism involves 66 species and 380 elementary reactions, and it can accurately predict the *ignition delay time*.	[15]
		2019	1000–2000 K / 0.10–5 MPa	A reduced mechanism includes 51 species and 420 reactions for $NH_3/CH_4/H_2$, and it showed over-prediction in *laminar burning velocities* of NH_3 and NH_3/CH_4 mixtures under fuel-rich conditions.	[14]
		2019	298 ± 3 K / 0.10–0.50 MPa	This study proposed a reaction mechanism that involves 42 species and 130 reactions based on the mechanisms of GRI-Mech 3.0 and Tian. The mechanism models the unstretched *laminar burning velocity* of and *species* in CH_4-NH_3-air flames with high precision.	[52]
		2009	200–6000 K / 4 kPa	This research presented a mechanism which includes 84 species and 703 reactions. The mechanisms can correctly predict the concentration profiles of the major *species* and *intermediates*.	[11]
		2009	937 K – 1773 K	The Mendiara and Glarborg's mechanism involves 97 species and 779 elementary reactions. It can effectively predict *NO and CO$_2$ emissions*.	[10]
Microscale	Microscale observables/events	/	3000 K / 48.2 atm	CH_4 addition affects the *reaction start time, kinetic energy, reaction pathways*, and *number of intermediates* in the NH_3 combustion.	This work
		2023	2400–3600 K / 24.1–482 atm	CH_4 addition affects the *collision frequency, reaction rate* and *reaction pathways of NO$_x$ formation* in the NH_3 combustion.	[20]
		2021	2400–3200 K	CH_4 addition affects the *oxidation of NH$_3$ reaction*, number of intermediate molecules (O_2, CO, CH_3, H_2, N_2 and H_2O) and *elementary reactions*.	[19]
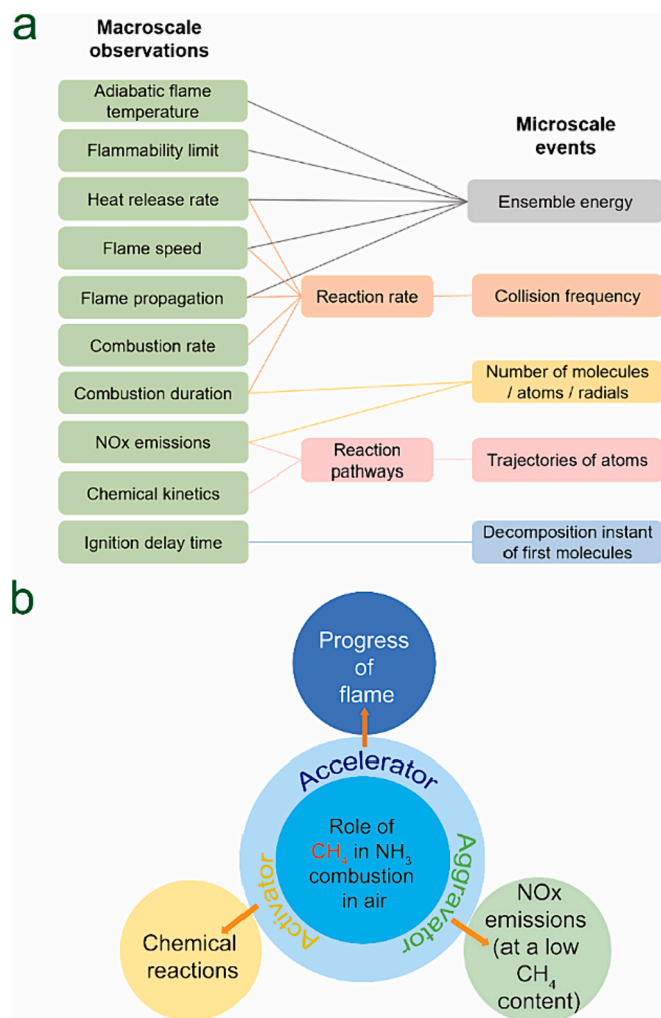
Fig. 8. Role of CH$_4$ in NH$_3$ combustion. a. A diagram linking the macroscale observations and microscale events. b. Role of CH$_4$ in NH$_3$ combustion.

Acknowledgement

References

[1] W.S. Chai, Y. Bao, P. Jin, G. Tang, L. Zhou, A review on ammonia, ammonia-hydrogen and ammonia-methane fuels, Renew. Sust. Energ. Rev. 147 (2021) 111254, https://doi.org/10.1016/j.rser.2021.111254.
[2] M. Zhang, X. Wei, J. Wang, Z. Huang, H. Tan, The blow-off and transient characteristics of co-firing ammonia/methane fuels in a swirl combustor, Proc. Combust. Inst. 38 (2021) 5181–5190, https://doi.org/10.1016/j.proci.2020.08.056.
[3] E.C. Okafor, K.D.K.A. Somarathne, R. Ratthanan, A. Hayakawa, T. Kudo, O. Kurata, N. Iki, T. Tsujimura, H. Furutani, H. Kobayashi, Control of NOx and other emissions in micro gas turbine combustors fuelled with mixtures of methane and ammonia, Combust. Flame 211 (2020) 406–416, https://doi.org/10.1016/j.combustflame.2019.10.012.
[4] P.F. Henshaw, T. D'Andrea, K.R.C. Mann, D.S.K. Ting, Premixed ammonia-methane-air combustion, Combust. Sci. Technol. 177 (2005) 2151–2170, https://doi.org/10.1080/00102200500240695.
[5] O. Kurata, N. Iki, T. Matsunuma, T. Inoue, T. Tsujimura, H. Furutani, H. Kobayashi, A. Hayakawa, Performances and emission characteristics of NH$_3$–air and NH$_3$–CH$_4$–air combustion gas-turbine power generations, Proc. Combust. Inst. 36 (2017) 3351–3359, https://doi.org/10.1016/j.proci.2016.07.088.
[6] B. Li, Y. He, Z. Li, A.A. Konnov, Measurements of NO concentration in NH$_3$-doped CH$_4$+air flames using saturated laser-induced fluorescence and probe sampling, Combust. Flame 160 (2013) 40–46, https://doi.org/10.1016/j.combustflame.2012.10.003.
[7] Ø. Skreiberg, P. Kilpinen, P. Glarborg, Ammonia chemistry below 1400 K under fuel-rich conditions in a flow reactor, Combust. Flame 136 (2004) 501–518, https://doi.org/10.1016/j.combustflame.2003.12.008.
[8] A.A. Konnov, J.D.J.C.S. Ruyck, Technology, Kinetic modeling of the thermal decomposition of ammonia, Combust. Sci. Technol. 152 (2000) 23–37, https://doi.org/10.1080/00102200008952125.
[9] G.P. Smith, D.M. Golden, M. Frenklach, N.W. Moriarty, B. Eiteneer, M. Goldenberg, C.T. Bowman, R.K. Hanson, S. Song, W.C. Gardiner, V.V.L. Jr, Z. Qin, GRI-Mech 3.0. http://www.me.berkeley.edu/gri_mech/.
[10] T. Mendiara, P. Glarborg, Ammonia chemistry in oxy-fuel combustion of methane, Combust. Flame 156 (2009) 1937–1949, https://doi.org/10.1016/j.combustflame.2009.07.006.
[11] Z. Tian, Y. Li, L. Zhang, P. Glarborg, F. Qi, An experimental and kinetic modeling study of premixed NH$_3$/CH$_4$/O$_2$/Ar flames at low pressure, Combust. Flame 156 (2009) 1413, https://doi.org/10.1016/j.combustflame.2009.03.005.
[12] P. Glarborg, J.A. Miller, B. Ruscic, S.J. Klippenstein, Modeling nitrogen chemistry in combustion, Prog. Energy Combust. Sci. 67 (2018) 31, https://doi.org/10.1016/j.pecs.2018.01.002.
[13] E.C. Okafor, Y. Naito, S. Colson, A. Ichikawa, T. Kudo, A. Hayakawa, H. Kobayashi, Experimental and numerical study of the laminar burning velocity of CH$_4$–NH$_3$–air premixed flames, Combust. Flame 187 (2018) 185–198, https://doi.org/10.1016/j.combustflame.2017.09.002.
[14] R. Li, A.A. Konnov, G. He, F. Qin, D. Zhang, Chemical mechanism development and reduction for combustion of NH$_3$/H$_2$/CH$_4$ mixtures, Fuel 257 (2019) 116059, https://doi.org/10.1016/j.fuel.2019.116059.
[15] Y. Jiang, A. Gruber, K. Seshadri, F. Williams, An updated short chemical-kinetic nitrogen mechanism for carbon-free combustion applications, Int. J. Energy Res. 44 (2020) 795–810, https://doi.org/10.1002/er.4891.
[16] H. Mikulčić, J. Baleta, X. Wang, J. Wang, F. Qi, F. Wang, Numerical simulation of ammonia/methane/air combustion using reduced chemical kinetics models, Int. J. Hydrog. Energy 46 (2021) 23548–23563, https://doi.org/10.1016/j.ijhydene.2021.01.109.
[17] B. Shu, X. He, C.F. Ramos, R.X. Fernandes, M. Costa, Experimental and modeling study on the auto-ignition properties of ammonia/methane mixtures at elevated pressures, Proc. Combust. Inst. 38 (2021) 261–268, https://doi.org/10.1016/j.proci.2020.06.291.
[18] Y. Guo, H. Shi, H. Liu, Y.Q. Xie, Y.L. Guan, Reactive molecular dynamics simulation and chemical kinetic modeling of ammonia/methane co-combustion, Fuel 354 (2023), https://doi.org/10.1016/j.fuel.2023.129341.
[19] Q. Zhang, L. Guo, X. Cai, S. Shan, K. Li, J. Zhao, Z. Zhou, Chemical effect of CH$_4$ on NH$_3$ combustion in an O$_2$/N$_2$ environment via ReaxFF, Energy Fuel 35 (2021) 10918–10928, https://doi.org/10.1021/acs.energyfuels.1c01016.
[20] J. Wang, X.Z. Jiang, K.H. Luo, Exploring reaction mechanism for ammonia/methane combustion via reactive molecular dynamics simulations, Fuel 331 (2023) 125806, https://doi.org/10.1016/j.fuel.2022.125806.
[21] C. Ashraf, A.C.T. van Duin, Extension of the ReaxFF combustion force field toward syngas combustion and initial oxidation kinetics, J. Phys. Chem. A 121 (2017) 1051–1068, https://doi.org/10.1021/acs.jpca.6b12429.
[22] K. Chenoweth, A.C. van Duin, W.A. Goddard, ReaxFF reactive force field for molecular dynamics simulations of hydrocarbon oxidation, J. Phys. Chem. A 112 (2008) 1040–1053, https://doi.org/10.1021/jp709896w.
[23] A.C.T. van Duin, S. Dasgupta, F. Lorant, W.A. Goddard, ReaxFF: a reactive force field for hydrocarbons, J. Phys. Chem. A 105 (2001) 9396–9409, https://doi.org/10.1021/jp004368u.
[24] L. Martínez, R. Andrade, E.G. Birgin, J.M. Martínez, PACKMOL: a package for building initial configurations for molecular dynamics simulations, J. Comput. Chem. 30 (2009) 2157–2164, https://doi.org/10.1002/jcc.21224.
[25] L. Zhang, S.V. Zybin, A.C.T. van Duin, S. Dasgupta, W.A. Goddard, E.M. Kober, Carbon cluster formation during thermal decomposition of octahydro-1,3,5,7-tetranitro-1,3,5,7-tetrazocine and 1,3,5-triamino-2,4,6-trinitrobenzene high explosives from ReaxFF reactive molecular dynamics simulations, J. Phys. Chem. A 113 (2009) 10619–10640, https://doi.org/10.1021/jp901353a.
[26] A. Strachan, A.C.T. van Duin, D. Chakraborty, S. Dasgupta, W.A. Goddard, Shock waves in high-energy materials: the initial chemical events in nitramine RDX, Phys. Rev. Lett. 91 (2003) 098301, https://doi.org/10.1103/PhysRevLett.91.098301.
[27] T.P. Senftle, S. Hong, M.M. Islam, S.B. Kylasa, Y. Zheng, Y.K. Shin, C. Junkermeier, R. Engel-Herbert, M.J. Janik, H.M. Aktulga, T. Verstraelen, A. Grama, A.C.T. van Duin, The ReaxFF reactive force-field: development, applications and future directions, NPJ Comput. Mater. 2 (2016) 15011, https://doi.org/10.1038/npjcompumats.2015.11.
[28] A. Strachan, E.M. Kober, A.C.T. van Duin, J. Oxgaard, W.A. Goddard, Thermal decomposition of RDX from reactive molecular dynamics, J. Chem. Phys. 122 (2005) 54502, https://doi.org/10.1063/1.1831277.
[29] X.Z. Jiang, K.H. Luo, Reactive and electron force field molecular dynamics simulations of electric field assisted ethanol oxidation reactions, Proc. Combust. Inst. 38 (2021) 6605–6613, https://doi.org/10.1016/j.proci.2020.06.318.
[30] R. Thompson, Shear flow near solids: epitaxial order and flow boundary conditions, Phys. Rev. A 41 (12) (1990) 6830–6837, https://doi.org/10.1103/PHYSREVA.41.6830.
[31] A.P. Thompson, H.M. Aktulga, R. Berger, D.S. Bolintineanu, W.M. Brown, P.S. Crozier, P.J.T. In Veld, A. Kohlmeyer, S.G. Moore, T.D. Nguyen, R. Shan, M.J. Stevens, J. Tranchida, C. Trott, S.J. Plimpton, LAMMPS - a flexible simulation tool for particle-based materials modeling at the atomic, meso, and continuum

scales, Comput. Phys. Commun. 271 (2022) 108171, https://doi.org/10.1016/j.cpc.2021.108171.

[32] W. Humphrey, A. Dalke, K. Schulten, VMD: visual molecular dynamics, J. Mol. Graph. 14 (1996) 33–38, https://doi.org/10.1016/0263-7855(96)00018-5.

[33] M. Dontgen, M.D. Przybylski-Freund, L.C. Kroger, W.A. Kopp, A.E. Ismail, K. Leonhard, Automated discovery of reaction pathways, rate constants, and transition states using reactive molecular dynamics simulations, J. Chem. Theory Comput. 11 (2015) 2517–2524, https://doi.org/10.1021/acs.jctc.5b00201.

[34] H. Xiao, A. Valera-Medina, P.J. Bowen, Study on premixed combustion characteristics of co-firing ammonia/methane fuels, Energy 140 (2017) 125–135, https://doi.org/10.1016/j.energy.2017.08.077.

[35] S. Li, S. Zhang, H. Zhou, Z. Ren, Analysis of air-staged combustion of NH_3/CH_4 mixture with low NOx emission at gas turbine conditions in model combustors, Fuel 237 (2019) 50–59, https://doi.org/10.1016/j.fuel.2018.09.131.

[36] N. Sullivan, A. Jensen, P. Glarborg, M.S. Day, J.F. Grcar, J.B. Bell, C.J. Pope, R. J. Kee, Ammonia conversion and NOx formation in laminar coflowing nonpremixed methane-air flames, Combust. Flame 131 (2002) 285–298, https://doi.org/10.1016/S0010-2180(02)00413-3.

[37] A. Valera-Medina, S. Morris, J. Runyon, D.G. Pugh, R. Marsh, P. Beasley, T. Hughes, Ammonia, methane and hydrogen for gas turbines, Energy Procedia 75 (2015) 118–123, https://doi.org/10.1016/j.egypro.2015.07.205.

[38] G.B. Ariemma, G. Sorrentino, R. Ragucci, M. de Joannon, P. Sabia, Ammonia/methane combustion: stability and NOx emissions, Combust. Flame 241 (2022) 112071, https://doi.org/10.1016/j.combustflame.2022.112071.

[39] H. Xiao, S. Lai, A. Valera-Medina, J. Li, J. Liu, H. Fu, Experimental and modeling study on ignition delay of ammonia/methane fuels, Int. J. Energy Res. 44 (2020) 6939–6949, https://doi.org/10.1002/er.5460.

[40] L. Dai, S. Gersen, P. Glarborg, A. Mokhov, H. Levinsky, Autoignition studies of NH_3/CH_4 mixtures at high pressure, Combust. Flame 218 (2020) 19–26, https://doi.org/10.1016/j.combustflame.2020.04.020.

[41] X. Zhang, J. Tian, Z. Cui, S. Xiong, S. Yin, Q. Wang, W. Long, Visualization study on the effects of pre-chamber jet ignition and methane addition on the combustion characteristics of ammonia/air mixtures, Fuel 338 (2023) 127204, https://doi.org/10.1016/j.fuel.2022.127204.

[42] M. Zhang, Z. An, X. Wei, J. Wang, Z. Huang, H. Tan, Emission analysis of the $CH_4/NH_3/air$ co-firing fuels in a model combustor, Fuel 291 (2021) 120135, https://doi.org/10.1016/j.fuel.2021.120135.

[43] T. Shu, Y. Xue, Z. Zhou, Z. Ren, An experimental study of laminar ammonia/methane/air premixed flames using expanding spherical flames, Fuel 290 (2021) 120003, https://doi.org/10.1016/j.fuel.2020.120003.

[44] E.C. Okafor, H. Yamashita, A. Hayakawa, K.D.K.A. Somarathne, T. Kudo, T. Tsujimura, M. Uchida, S. Ito, H. Kobayashi, Flame stability and emissions characteristics of liquid ammonia spray co-fired with methane in a single stage swirl combustor, Fuel 287 (2021) 119433, https://doi.org/10.1016/j.fuel.2020.119433.

[45] J.W. Ku, Y.J. Ahn, H.K. Kim, Y.H. Kim, O.C. Kwon, Propagation and emissions of premixed methane-ammonia/air flames, Energy 201 (2020) 117632, https://doi.org/10.1016/j.energy.2020.117632.

[46] H. Xiao, S. Lai, A. Valera-Medina, J. Li, J. Liu, H. Fu, Study on counterflow premixed flames using high concentration ammonia mixed with methane, Fuel 275 (2020) 117902, https://doi.org/10.1016/j.fuel.2020.117902.

[47] X. Han, Z. Wang, M. Costa, Z. Sun, Y. He, K. Cen, Experimental and kinetic modeling study of laminar burning velocities of NH_3/air, $NH_3/H_2/air$, $NH_3/CO/air$ and $NH_3/CH_4/air$ premixed flames, Combust. Flame 206 (2019) 214–226, https://doi.org/10.1016/j.combustflame.2019.05.003.

[48] K.D.K.A. Somarathne, E.C. Okafor, D. Sugawara, A. Hayakawa, H. Kobayashi, Effects of OH concentration and temperature on NO emission characteristics of turbulent non-premixed CH4/NH3/air flames in a two-stage gas turbine like combustor at high pressure, Proc. Combust. Inst. 38 (2021) 5163–5170, https://doi.org/10.1016/j.proci.2020.06.276.

[49] R.C. Rocha, S. Zhong, L. Xu, X.-S. Bai, M. Costa, X. Cai, H. Kim, C. Brackmann, Z. Li, M. Aldén, Structure and laminar flame speed of an ammonia/methane/air premixed flame under varying pressure and equivalence ratio, Energy Fuel 35 (2021) 7179–7192, https://doi.org/10.1021/acs.energyfuels.0c03520.

[50] E.C. Okafor, O. Kurata, H. Yamashita, T. Inoue, T. Tsujimura, N. Iki, A. Hayakawa, S. Ito, M. Uchida, H. Kobayashi, Liquid ammonia spray combustion in two-stage micro gas turbine combustors at 0.25 MPa; relevance of combustion enhancement to flame stability and NOx control, Appl. Energy Combust. Sci. 7 (2021) 100038, https://doi.org/10.1016/j.jaecs.2021.100038.

[51] M. Zhang, Z. An, L. Wang, X. Wei, B. Jianayihan, J. Wang, Z. Huang, H. Tan, The regulation effect of methane and hydrogen on the emission characteristics of ammonia/air combustion in a model combustor, Int. J. Hydrog. Energy 46 (2021) 21013–21025, https://doi.org/10.1016/j.ijhydene.2021.03.210.

[52] E.C. Okafor, Y. Naito, S. Colson, A. Ichikawa, T. Kudo, A. Hayakawa, H. Kobayashi, Measurement and modelling of the laminar burning velocity of methane-ammonia-air flames at high pressures using a reduced reaction mechanism, Combust. Flame 204 (2019) 162–175, https://doi.org/10.1016/j.combustflame.2019.03.008.